# Multiplexed and portable nucleic acid detection platform with Cas13, Cas12a, and Csm6

Jonathan S. Gootenberg,[1,2,3,4,5]* Omar O. Abudayyeh,[1,2,3,4,6]* Max J. Kellner,[1] Julia Joung,[1,2,3,4] James J. Collins,[1,4,6,7,8] Feng Zhang[1,2,3,4]†

Rapid detection of nucleic acids is integral for clinical diagnostics and biotechnological applications. We recently developed a platform termed SHERLOCK (specific high-sensitivity enzymatic reporter unlocking) that combines isothermal preamplification with Cas13 to detect single molecules of RNA or DNA. Through characterization of CRISPR enzymology and application development, we report here four advances integrated into SHERLOCK version 2 (SHERLOCKv2) (i) four-channel single-reaction multiplexing with orthogonal CRISPR enzymes; (ii) quantitative measurement of input as low as 2 attomolar; (iii) 3.5-fold increase in signal sensitivity by combining Cas13 with Csm6, an auxiliary CRISPR-associated enzyme; and (iv) lateral-flow readout. SHERLOCKv2 can detect Dengue or Zika virus single-stranded RNA as well as mutations in patient liquid biopsy samples via lateral flow, highlighting its potential as a multiplexable, portable, rapid, and quantitative detection platform of nucleic acids.

Versatile, rapid, and portable sensing of nucleic acids is vital for applications in human health. The RNA-targeting CRISPR-associated enzyme Cas13 (*1, 2*) has recently been adapted for such purpose. This detection platform, termed SHERLOCK (specific high-sensitivity enzymatic reporter unlocking) (*3*), can discriminate between inputs that differ by a single nucleotide at very low concentrations and can be lyophilized for portable deployment. However, this technology has several limitations, including the lack of quantitation and reliance on fluorescence detection equipment for readout. Here, we extend the SHERLOCK technology to address these limitations and further develop the utility of this platform.

Many applications require detection of more than one target molecule in a single reaction, and we therefore sought to create a multiplexed platform that relies on specific cleavage preferences of Cas enzymes (*2–5*). To identify possible candidate enzymes compatible with multiplexing, we biochemically characterized three members of the CRISPR-Cas13a family and 14 members of the CRISPR-Cas13b family (*6, 7*) (figs. S1 and S2 and table S1). We profiled cleavage preferences on homopolymer reporters and found that most orthologs preferred either uridine, a combination of bases, or adenine (fig. S3 and

tables S2 to S5) and that cleavage could be improved with buffer and CRISPR RNA (crRNA) design optimization (figs. S4 to S7 and supplementary methods). Among the adenine-cleaving enzymes, Cas13b from *Prevotella* sp. MA2016 (PsmCas13b) was more sensitive than Cas13a from *Lachnospiraceae* bacterium NK4A179 (LbaCas13a) (fig. S8). We refined the cleavage sequence preferences by evaluating collateral activity across dinucleotide motifs (Fig. 1A), finding a large diversity of dinucleotide cleavage motif preferences (figs. S9 and S10 and supplementary methods). From these dinucleotide cleavage screens, we found that the activities of LwaCas13a, Cas13b from *Capnocytophaga canimorsus* Cc5 (CcaCas13b), LbaCas13a, and PsmCas13b could all be independently measured with the four dinucleotide reporters AU, UC, AC, and GA, respectively (Fig. 1B and fig. S11). Additionally, using a random in vitro RNA library motif cleavage screen, we identified numerous RNA oligomers of 6 bases that allowed for further orthogonality between Cas13 enzymes (figs. S12 to S15 and supplementary methods).

Using these specific cleavage preferences, we could detect synthetic Zika virus (ZIKV) ssRNA in the HEX channel and synthetic Dengue virus (DENV) ssRNA in the FAM channel in the same reaction (fig. S16). To expand the in-sample multiplexing capabilities of SHERLOCK, we engineered a detection system based on Cas12a (Cpf1), which also exhibits collateral activity (*8*) (Fig. 1C). Although Cas12a from *Acidaminococcus* sp. BV3L6 (AsCas12a) collateral activity did not produce a detectable signal at input concentrations <10 nM, preamplification with recombinase polymerase amplification (RPA) enabled single-molecule detection at 2 aM (Fig. 1D and fig. S17) (unless otherwise noted, all SHERLOCK reactions that involve preamplification are performed in two steps, with the RPA reaction mixture being

directly added to the Cas13 assay without any purification step). For triplex detection, we designed a LwaCas13a uridine reporter in the Cy5 channel, a PsmCas13b adenine reporter in the FAM channel, and an AsCas12a ssDNA reporter in the HEX channel (fig. S18A). We were able to detect three targets (a synthetic ssDNA target, ZIKV ssRNA, and DENV ssRNA) in a single reaction (fig. S18B). We further extended detection to four targets by leveraging orthogonal dinucleotide motifs, with reporters for LwaCas13a, PsmCas13b, CcaCas13b, and AsCas12a in FAM, TEX, Cy5, and HEX channels, respectively (Fig. 1E), and could distinguish all combinations of targets (Fig. 1F). When combined with RPA, we detected two DNA targets (the *Pseudomonas aeruginosa* acyltransferase gene and the *Staphylococcus aureus* thermonuclease gene) (Fig. 1G) at concentrations as low as the attomolar range (Fig. 1H). Similarly, multiplexed SHERLOCK with PsmCas13b and LwaCas13a achieved attomolar multiplexed detection of ZIKV and DENV RNA dilutions as well as allele-specific genotyping of human saliva samples (fig. S19). These advances on in-sample multiplexing via orthogonal base preferences allow for many targets to be detected at scale and for cheaper cost.

We next focused on tuning the output of the SHERLOCK signal to make it more quantitative, sensitive, and robust to broaden the utility of the technology. SHERLOCK relies on an exponential preamplification, which saturates quickly and hinders accurate quantitation, but we observed that more dilute primer concentrations increased both raw signal and quantitative accuracy, indicating that at lower primer concentrations, the reaction does not saturate (Fig. 2, A and B, and fig. S20, A to E). We tested a range of primer concentrations and found that 240 nM exhibited the greatest correlation between signal and input (fig. S20F), and quantitation was sustainable across a large range of sample concentrations as low as the attomolar range (Fig. 2C and fig. S20G). Many applications of nucleic acid detection, such as HIV detection (*9, 10*), require single-molecule-per-milliliter sensitivity, and we therefore tested whether the detection limit could be pushed beyond 2 aM, allowing for more dilute sample inputs into SHERLOCK. By scaling up the preamplification RPA step, we found that LwaCas13a could produce a detection signal for 200, 80, and 8 zM input samples and allow for single-molecule volume inputs of 250 and 540 μl (fig. S21, A and B), and PsmCas13b could detect 200 zM input samples in 250-μl reactions (fig. S21C).

To amplify the detection signal, we leveraged the CRISPR type III effector nuclease Csm6 (*11–17*), which is activated by cyclic adenylate molecules or linear adenine homopolymers terminated with a 2′,3′-cyclic phosphate (*18, 19*). LwaCas13a and PsmCas13b collateral activity generates cleavage products with hydroxylated 5′ ends and 2′,3′-cyclic phosphate ends (fig. S22), suggesting that Cas13 collateral activity could generate Csm6 activating species, which would allow for amplified signal detection in the SHERLOCK

[1]Broad Institute of the Massachusetts Institute of Technology (MIT) and Harvard, Cambridge, MA 02142, USA. [2]McGovern Institute for Brain Research, MIT, Cambridge, MA 02139, USA. [3]Department of Brain and Cognitive Science, MIT, Cambridge, MA 02139, USA. [4]Department of Biological Engineering, MIT, Cambridge, MA 02139, USA. [5]Department of Systems Biology, Harvard University, Boston, MA 02115, USA. [6]Department of Health Sciences and Technology, MIT, Cambridge, MA 02139, USA. [7]Institute for Medical Engineering and Science, MIT, Cambridge, MA 02139, USA. [8]Wyss Institute for Biologically Inspired Engineering, Harvard University, Boston, MA 02115, USA.
*These authors contributed equally to this work.
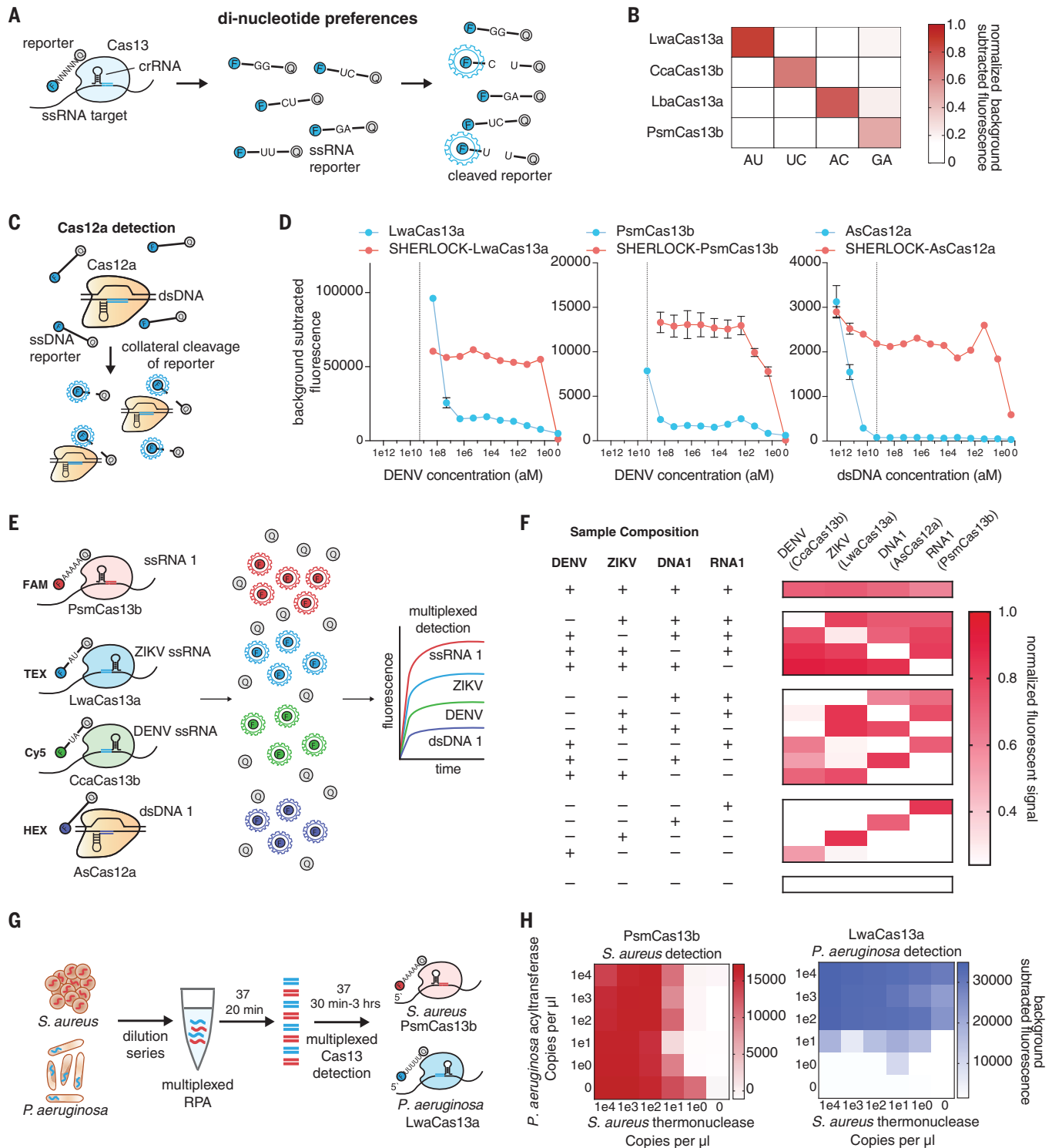†Corresponding author. Email: zhang@broadinstitute.org

**Fig. 1. Multiplexed SHERLOCK detection with orthogonal collateral activity of class 2 enzymes.** (**A**) Schematic of assay for determining dinucleotide preferences of Cas13a/b enzymes. (**B**) Collateral activity of LwaCas13a, CcaCas13b, LbaCas13a, and PsmCas13b on orthogonal dinucleotide reporters. (**C**) Schematic of collateral activity of Cas12a activated by double-stranded DNA (dsDNA). (**D**) Comparison of collateral activity and preamplification enhanced collateral activity (SHERLOCK) of LwaCas13a, PsmCas13b, and AsCas12a. The dotted line denotes 2e9 (aM), the limit of AsCas12a sensitivity without preamplification.

Values represent mean ± SEM. (**E**) Schematic of in-sample four-channel multiplexing with orthogonal Cas13 and Cas12a enzymes. (**F**) In-sample multiplexed detection of ZIKV ssRNA, ssRNA 1, DENV ssRNA, and dsDNA 1 with LwaCas13a, PsmCas13b, CcaCas13b, and AsCas12a, respectively. (**G**) Schematic of in-sample multiplexed detection of *S. aureus* thermonuclease and *P. aeruginosa* acyltransferase synthetic targets with LwaCas13a and PsmCas13b. (**H**) In-sample multiplexed RPA and collateral detection at decreasing concentrations of *S. aureus* thermonuclease and *P. aeruginosa* acyltransferase synthetic targets with LwaCas13a and PsmCas13b.

assay. By testing RNA adenylate molecules of different lengths and 3′-end modifications (figs. S23 and S24A and table S6), we found that Csm6 from *Enterococcus italicus* (EiCsm6) and Csm6 from *Lactobacillus salivarius* (LsCsm6) were efficiently activated by hexadenylates containing 2′,3′-cyclic phosphate ends (fig. S24, B and C). Moreover, EiCsm6, LsCsm6, and Csm6 from *Thermus thermophilus* (TtCsm6) demonstrated a strong cleavage preference for A- and C-rich reporters based on reporter screening, enabling independent measurements of LwaCas13a and Csm6 cleavage activity in separate channels (Fig. 2D and figs. S24, B to D, S25, and S26, A to E).

To couple the activity of Cas13 with Csm6 activation, we designed protected RNA activators that contained a polyadenylate [poly(A)] stretch followed by a protecting poly(U) stretch that could be cleaved by a uracil-preferring Cas13 enzyme, with the rationale that LwaCas13a could degrade all the uridines down to the homopolymeric A stretch because it had robust activity on UU and AU two-base motifs (fig. S9). We found that, upon addition of target and LwaCas13a-crRNA complex, EiCsm6 and LsCsm6 were activated by the $(A)_6$-$(U)_5$ activator, con-

sistent with the finding that the $A_6$ activator is optimal for Csm6 activation and confirmed by mass spectrometry (Fig. 2E and figs. S26F, S27, and S28). We combined the reporters for both Csm6 and Cas13 in the same reaction within the same fluorescence channel and found that increasing the activator concentration increased the synergistic activation of Csm6 by Cas13 for DENV ssRNA detection (Fig. 2F), and that increasing the Csm6-specific poly(A) reporter also increased the Csm6 signal, leading to a larger increase in signal upon activator addition (fig. S29, A and B). After optimization (fig. S30), we found that Csm6-enhanced LwaCas13a increased the overall signal and kinetics of synthetic acyltransferase gene detection by SHERLOCK (Fig. 2G).

Another goal of SHERLOCKv2 was engineering a visual readout of activity requiring no additional instrumentation. We first tested a colorimetric ribonuclease (RNase) reporter based on gold nanoparticle cluster disaggregation (*20, 21*), but this readout required a level of RNase activity beyond what Cas13 collateral activity could achieve (fig. S31). We then designed a lateral-flow readout that was based on the destruction of a FAM-biotin reporter, allowing for

detection on commercial lateral flow strips. Abundant reporter accumulates anti-FAM antibody-gold nanoparticle conjugates at the first line on the strip, preventing binding of the antibody-gold conjugates to protein A on the second line; cleavage of reporter would reduce accumulation at the first line and result in signal on the second line (Fig. 3A). We tested this design for instrument-free detection of ZIKV or DENV ssRNA and found that detection was possible in <90 min with sensitivities as low as 2 aM (Fig. 3, B and C, and fig. S32). Moreover, we found that we could do rapid (<10 min) genomic DNA extraction from human saliva and input this directly into SHERLOCK without purification for rapid genotyping in <23 min by fluorescence and 2 hours by lateral flow (fig. S33). This exemplifies a closed-tube assay format in which the entire SHERLOCK reaction is performed in a one-pot assay without any sample purification.

We also applied the system to create a rapid and portable paper test for detecting mutations in liquid biopsies of non–small cell lung cancer (NSCLC) patients. We designed SHERLOCK assays to detect either the epidermal growth factor receptor (EGFR) Leu→Arg (L858R) mutation or
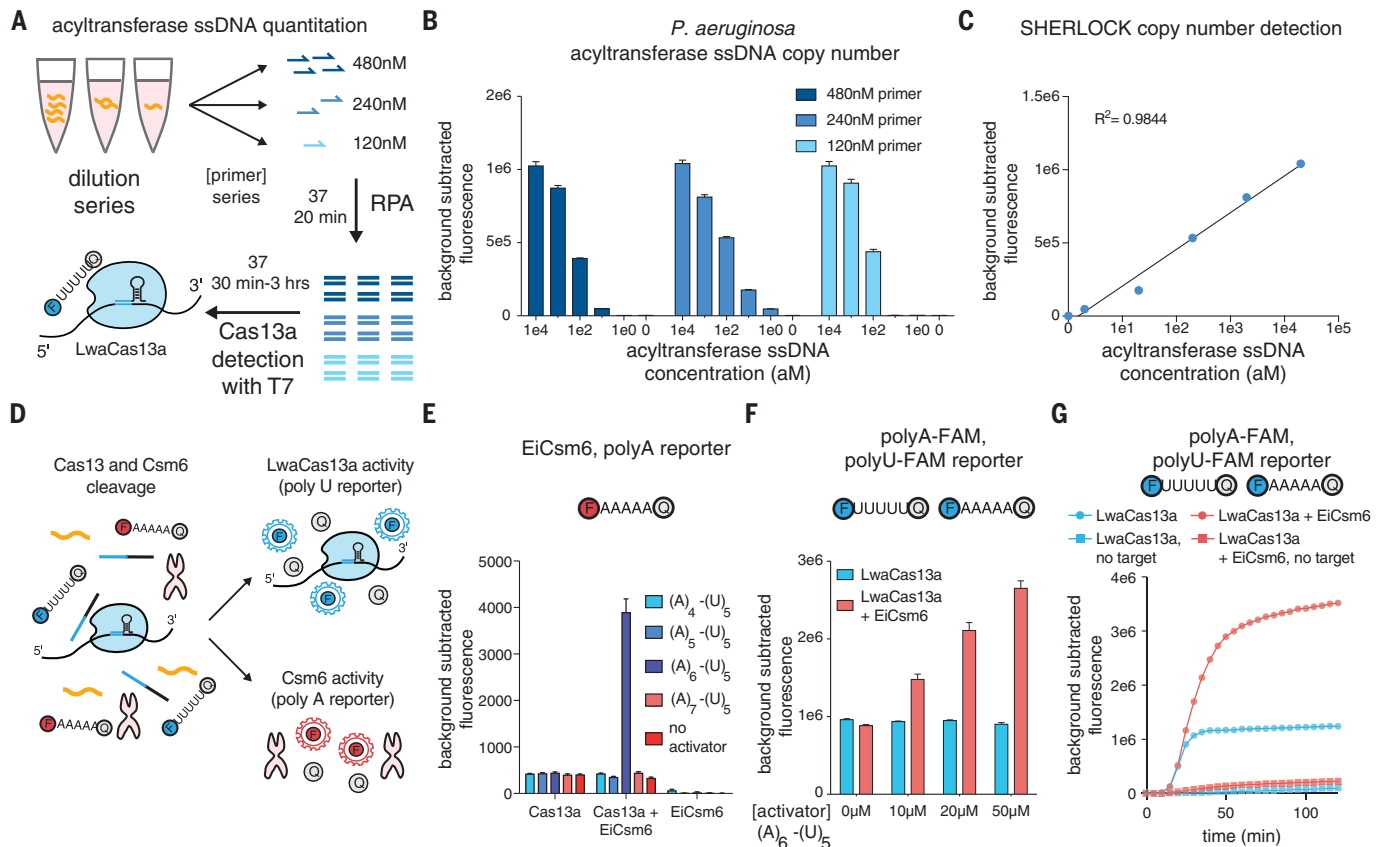
**Fig. 2. Single-molecule quantitation and enhanced signal with SHERLOCK and Csm6.** (**A**) Schematic of DNA reaction scheme for quantitation of *P. aeruginosa* synthetic DNA. (**B**) Quantitation of *P. aeruginosa* synthetic DNA at various RPA primer concentrations. Values represent mean ± SEM. (**C**) Correlation of *P. aeruginosa* synthetic DNA concentration with detected fluorescence. Values represent mean ± SEM. (**D**) Schematic of independent readout of LwaCas13a and Csm6 cleavage activity with

orthogonal reporters. (**E**) Activation of EiCsm6 by LwaCas13a cleavage of adenine-uridine activators with adenine tracts of different lengths. LwaCas13a is targeting synthetic DENV ssRNA. Values represent mean ± SEM. (**F**) Combined LwaCas13a and EiCsm6 signal for increasing concentrations of $(A)_6$-$(U)_5$ activator detecting 20 nM of DENV ssRNA. Values represent mean ± SEM. (**G**) Kinetics of EiCsm6-enhanced LwaCas13a SHERLOCK detection of *P. aeruginosa* acyltransferase synthetic target.

the exon 19 deletion (five amino acids) and isolated cell-free DNA (cfDNA) from patients with or without these mutations (Fig. 3D), as verified by targeted sequencing (table S7). SHERLOCK successfully detected these mutations, both with fluorescence-based readout (Fig. 3, E and H)

and lateral flow–based readout (Fig. 3, F, G, I, and J, and fig. S34, A to D). Fluorescence-based SHERLOCK could also detect a different common EGFR mutation, Thr→Met (T790M), in synthetic and patient cfDNA liquid biopsy samples (fig. S34, E and F).

To improve the robustness of the detection and reduce the likelihood of a false-positive readout, we combined Csm6 with Cas13 detection on lateral flow (Fig. 3K). We tested lateral-flow reporters of various sequences and lengths in the presence of Csm6 and activator and found
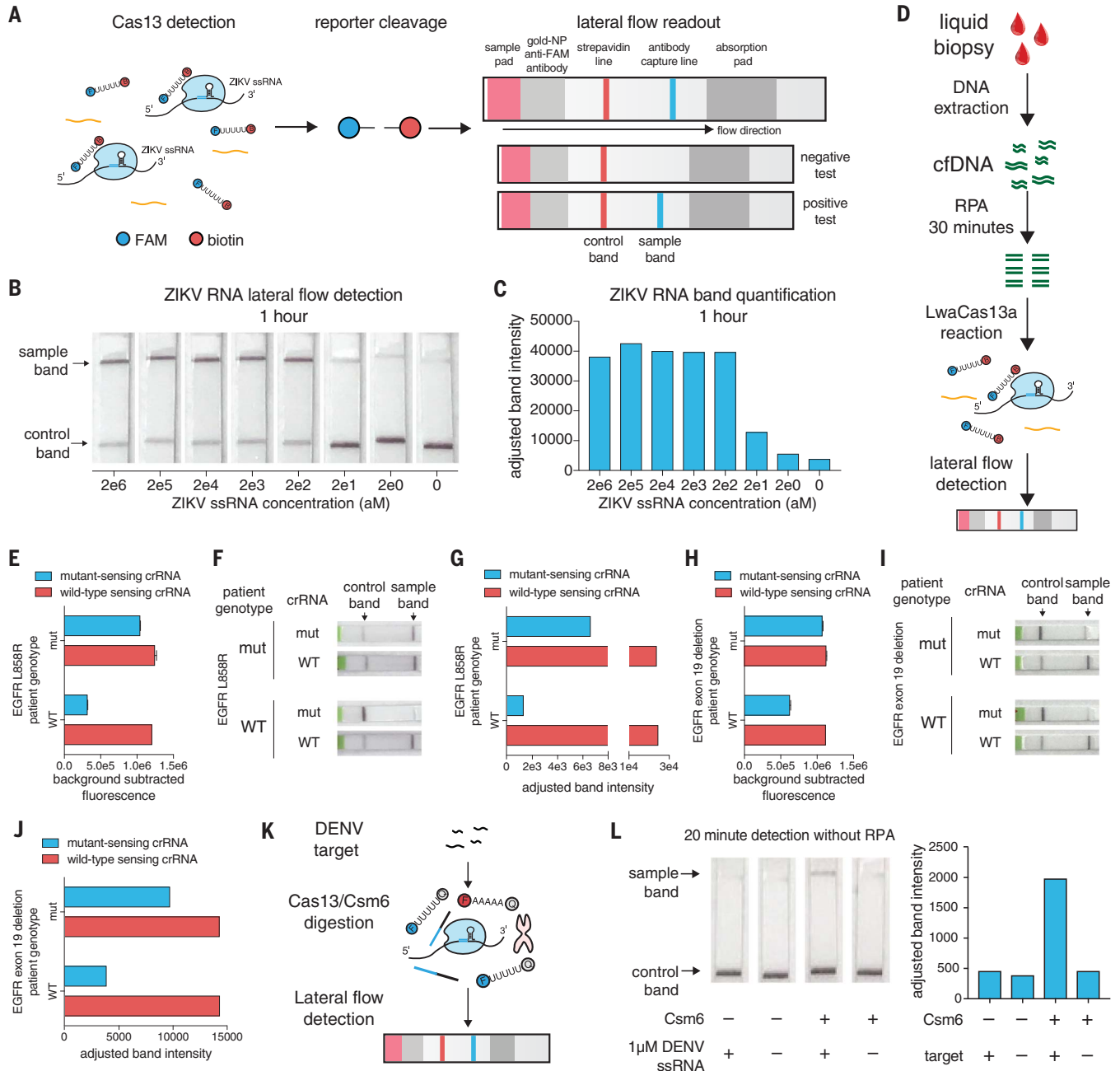


**Fig. 3. Adapting SHERLOCK for lateral flow detection.** (**A**) Schematic of lateral-flow detection with SHERLOCK. (**B**) Detection of synthetic ZIKV ssRNA using lateral-flow SHERLOCK with 1 hour of LwaCas13a reaction. (**C**) Quantitation of band intensity from detection in (B). (**D**) Schematic of lateral flow detection of therapeutically relevant EGFR mutations from patient liquid biopsy samples. (**E**) Detection of EGFR L858R mutation in patient-derived cfDNA samples with either L858R or wild-type (WT) alleles. Values represent mean ± SEM. (**F**) Lateral-flow detection of EGFR L858R mutation in patient-derived cfDNA samples with either L858R or WT alleles.

(**G**) Quantitation of band intensity from detection in (E). (**H**) Detection of EGFR exon 19 deletion mutation in patient-derived cfDNA samples with either exon 19 deletion or WT alleles. Values represent mean ± SEM. (**I**) Lateral-flow detection of EGFR exon 19 deletion mutation in patient-derived cfDNA samples with either exon 19 deletion or WT alleles. (**J**) Quantitation of band intensity from detection in (H). (**K**) Schematic of lateral-flow readout of EiCsm6-enhanced LwaCas13a detection of DENV ssRNA. (**L**) EiCsm6-enhanced lateral-flow detection of synthetic DENV RNA in combination with LwaCas13a without preamplification by RPA. Band intensity quantitation is shown to the right.

that a long A-C reporter demonstrated strong cleavage signal (fig. S35, A and B). We used this reporter in combination with the Cas13 lateral-flow reporter for rapid detection of DENV ssRNA, relying solely on Csm6 for amplification (i.e., in the absence of RPA) (Fig. 3L). We subsequently combined RPA, Cas13/Csm6, and lateral-flow readout to detect an acyltransferase target and found that the increase in signal conferred by Csm6 allowed for more rapid detection by lateral flow (fig. S35, C and D) with reduced background.

Finally, we applied SHERLOCKv2 in a simulated approach that involves Cas13 serving as both a companion diagnostic and the therapy itself, as Cas13 has been developed for a variety of applications in mammalian cells, including RNA knockdown, imaging, and editing (22, 23) (Fig. 4A and table S8). We recently harnessed Cas13b from *Prevotella* sp. P5-125 (PspCas13b) to correct mutations underlying genetic diseases by using a system called RNA Editing for Programmable A-to-I Replacement (REPAIR) (23). To direct and monitor the outcome of a treatment, we tested if SHERLOCK could be used both for genotyping to inform the REPAIR treatment and as a readout of the edited RNA to track the efficiency of the therapy. We used a mutation in *APC* (APC:c.1262G>A) implicated in familial adenomatous polyposis 1 (Fig. 4, B and C) (24) and transfected synthetic healthy and mutant cDNAs of the fragment surrounding the mutation into human embryonic kidney (HEK) 293FT cells. We harvested DNA from these cells and successfully genotyped the correct samples by using single-sample multiplexed SHERLOCK with LwaCas13a and PsmCas13b (Fig. 4D). Concurrently, we designed and cloned guide RNAs for the REPAIR system and transfected cells that had the diseased genotype with the guide RNA and dPspCas13b-ADAR2$_{dd}$(E488Q) REPAIR system. We confirmed editing by next-generation sequencing analysis, finding that 43% editing was achieved with the REPAIR system (Fig. 4E), and we could detect this editing with SHERLOCK (Fig. 4F and fig. S36).

The additional refinements presented here for Cas13-based detection allow for quantitative, visual, more sensitive, and multiplexed readouts, enabling additional applications for nucleic acid detection, especially in settings where portable and instrument-free analysis is necessary (table S9). SHERLOCKv2 can be used for multiplexed genotyping to inform pharmacogenomic therapeutic development and application, detecting genetically modified organisms in the field, or determining the presence of co-occurring pathogens. Moreover, the rapid, isothermal readout of SHERLOCKv2, enabled by lateral flow and Csm6, provides an opportunity for detection in settings where power or portable readers are unavailable, even for rare species like circulating DNA. In the future, it might be possible to make solution-based colorimetric readouts and multiplex lateral-flow assays containing multiple test lines for different targets. Improved CRISPR-based diagnostic (CRISPR-dx) nucleic acid tests make it easier
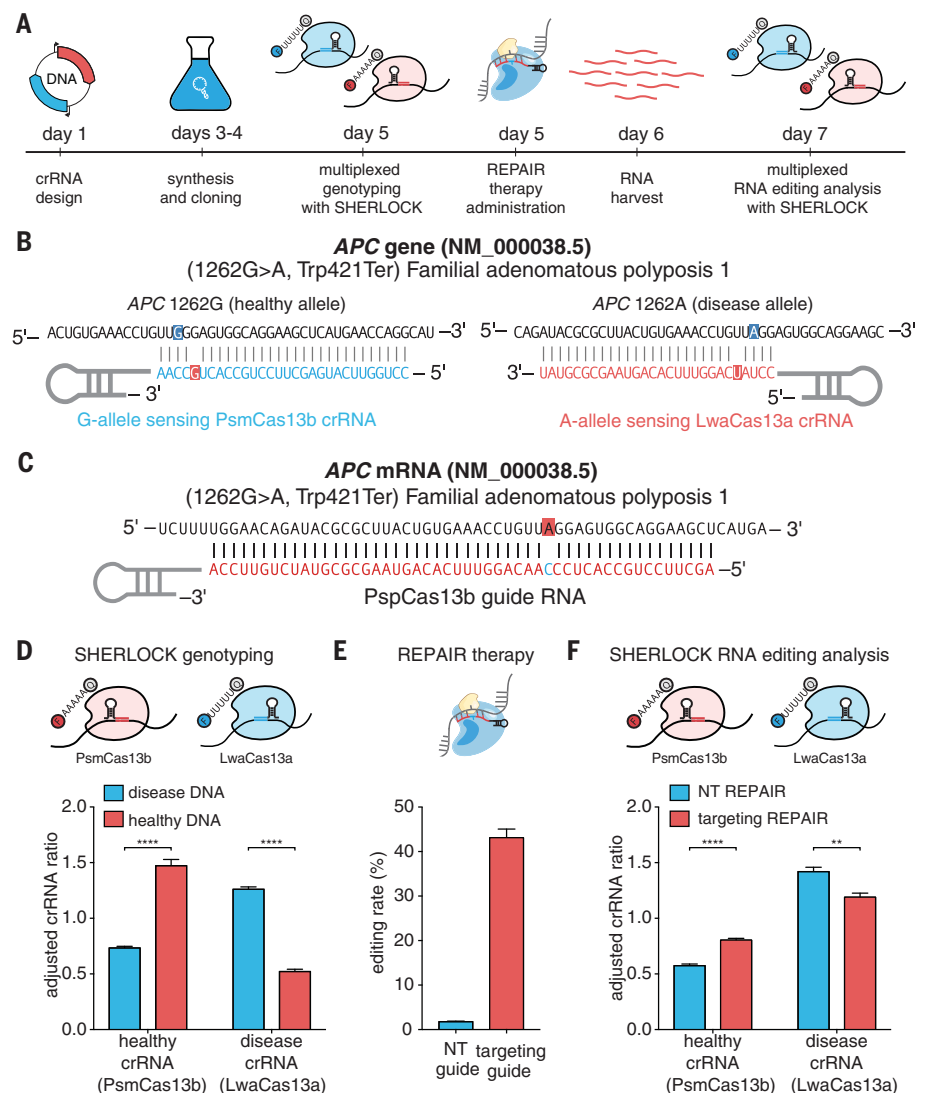
to detect the presence of nucleic acids in a range of applications across biotechnology and health and are now field-ready for rapid and portable deployment.



**Fig. 4. Combined therapeutics and diagnostics with Cas13 enzymes.** (**A**) Schematic of time line for detection of disease alleles, correction with REPAIR, and assessment of REPAIR correction. (**B**) Sequences of targets and crRNA designs used for detection of *APC* alleles. (**C**) Sequences of target and REPAIR guide design used for correction of *APC* alleles. (**D**) In-sample multiplexed detection of *APC* alleles from healthy- and disease-simulating samples with LwaCas13a and PsmCas13b. Adjusted crRNA ratio allows for comparisons between different crRNAs that will have different overall signal levels (see supplementary methods for more details). Values represent mean ± SEM. (**E**) Quantitation of REPAIR editing efficiency at the targeted *APC* mutation. Values represent mean ± SEM. (**F**) In-sample multiplexed detection of *APC* alleles from REPAIR targeting and nontargeting samples with LwaCas13a and PsmCas13b. Values represent mean ± SEM.

**REFERENCES AND NOTES**
1. S. Shmakov *et al.*, *Mol. Cell* **60**, 385–397 (2015).
2. O. O. Abudayyeh *et al.*, *Science* **353**, aaf5573 (2016).
3. J. S. Gootenberg *et al.*, *Science* **356**, 438–442 (2017).
4. A. East-Seletsky *et al.*, *Nature* **538**, 270–273 (2016).
5. A. East-Seletsky, M. R. O'Connell, D. Burstein, G. J. Knott, J. A. Doudna, *Mol. Cell* **66**, 373–383.e3 (2017).
6. S. Shmakov *et al.*, *Nat. Rev. Microbiol.* **15**, 169–182 (2017).
7. A. A. Smargon *et al.*, *Mol. Cell* **65**, 618–630.e7 (2017).
8. J. S. Chen, E. Ma, L. B. Harrington, X. Tian, J. A. Doudna, *bioRxiv* [preprint]. 29 November 2017. www.biorxiv.org/content/early/2017/11/29/226993.
9. W. H. Organization, in *Guidelines for Using HIV Testing Technologies in Surveillance: Selection, Evaluation and Implementation: 2009 Update* (Geneva, 2009).
10. J. M. Barletta, D. C. Edelman, N. T. Constantine, *Am. J. Clin. Pathol.* **122**, 20–27 (2004).
11. L. Deng, R. A. Garrett, S. A. Shah, X. Peng, Q. She, *Mol. Microbiol.* **87**, 1088–1099 (2013).
12. G. W. Goldberg, W. Jiang, D. Bikard, L. A. Marraffini, *Nature* **514**, 633–637 (2014).
13. W. Jiang, P. Samai, L. A. Marraffini, *Cell* **164**, 710–721 (2016).
14. O. Niewoehner, M. Jinek, *RNA* **22**, 318–329 (2016).
15. P. Samai *et al.*, *Cell* **161**, 1164–1174 (2015).
16. R. H. Staals *et al.*, *Mol. Cell* **56**, 518–530 (2014).
17. G. Tamulaitis *et al.*, *Mol. Cell* **56**, 506–517 (2014).

18. M. Kazlauskiene, G. Kostiuk, Č. Venclovas, G. Tamulaitis, V. Siksnys, *Science* **357**, 605–609 (2017).
19. O. Niewoehner *et al.*, *Nature* **548**, 543–548 (2017).
20. W. Zhao, M. M. Ali, S. D. Aguirre, M. A. Brook, Y. Li, *Anal. Chem.* **80**, 8431–8437 (2008).
21. W. Zhao, J. C. Lam, W. Chiuman, M. A. Brook, Y. Li, *Small* **4**, 810–816 (2008).
22. O. O. Abudayyeh *et al.*, *Nature* **550**, 280–284 (2017).
23. D. B. T. Cox *et al.*, *Science* **358**, 1019–1027 (2017).
24. S. Cottrell, W. F. Bodmer, D. Bicknell, L. Kaklamanis, *Lancet* **340**, 626–630 (1992).

## SUPPLEMENTARY MATERIALS

www.sciencemag.org/content/360/6387/439/suppl/DC1
Materials and Methods
Figs. S1 to S36
Tables S1 to S8
References (*25–27*)

# Science

## Multiplexed and portable nucleic acid detection platform with Cas13, Cas12a, and Csm6

Jonathan S. Gootenberg, Omar O. Abudayyeh, Max J. Kellner, Julia Joung, James J. Collins and Feng Zhang

**Taking CRISPR technology further**
        CRISPR techniques are allowing the development of technologies for nucleic acid detection (see the Perspective by Chertow). Taking advantages of the distinctive enzymatic properties of CRISPR enzymes, Gootenberg  *et al.* developed an improved nucleic acid detection technology for multiplexed quantitative and highly sensitive detection, combined with lateral flow for visual readout. Myhrvold *et al.* added a sample preparation protocol to create a field-deployable viral diagnostic platform for rapid detection of specific strains of pathogens in clinical samples. Cas12a (also known as Cpf1), a type V CRISPR protein, cleaves double-stranded DNA and has been adapted for genome editing. Chen  *et al.* discovered that Cas12a also processes single-stranded DNA threading activity. A technology platform based on this activity detected human papillomavirus in patient samples with high sensitivity.
        *Science*, this issue p. 439, p. 444, p. 436; see also p. 381